**Trends in**
Chemical Physics
Vol. 12, 2005

Review

# The spectroscopic and dissociation dynamics studies of triatomic molecular ions

**Limin Zhang[a], Shilin Liu[b], Shuqin Yu, Jinghua Dai and Xingxiao Ma**
Department of Chemical Physics, University of Science and Technology of China, Hefei, Anhui 230026, P. R. China

## ABSTRACT

The recent research results about the photo-fragment excitation (PHOFEX) spectrum and the dissociation dynamics of the triatomic molecular ions ($CS_2^+$, $SO_2^+$, $N_2O^+$) are reviewed. The parent ions with state selectivity are prepared via resonance-enhanced multi-photon ionization (REMPI) of neutral molecules using a tunable pulsed laser, and then the parent ions are photodissociated with another laser overlapping temporally and spatially with the first laser. The PHOFEX spectrum is obtained by monitoring the variation of fragment ion signal intensity versus dissociation laser wavelength. From the PHOFEX spectrum the spectroscopic and dissociation information of $CS_2^+$, $SO_2^+$, $N_2O^+$ were derived.

**KEYWORDS:** $CS_2^+$, $SO_2^+$, $N_2O^+$, REMPI, PHOFEX spectrum

## I. INTRODUCTION

Photodissociation of molecules lies at the heart of spectroscopy and photochemistry. Besides its practical importance, experimental studies of molecular photodissociation often provide useful information on the intra- and intermolecular dynamics or, more specifically, the curve crossing, interference, spin-orbit coupling between the electronic states, the energy transfer from one mode to the others, and the breaking of bonds to form fragment products, etc. The development of sophisticated new experimental methods, often involving several lasers, has made it possible to study the fragmentation mechanism of unstable molecules (free radicals, molecular ions) in unprecedented presion (high resolution spectra and mass selected).

This paper will review the recent development on the photodissociation of some triatomic ions ($CS_2^+$, $SO_2^+$, $N_2O^+$) which play important roles in astrophysics, atmospheric chemistry, environmental pollution, and industry [1-5].

### I-1. The preparation of molecular ions with state selected

Different from the "indirect" method, such as the photoionization or photoelectron spectrum of molecules, a "direct" method to study molecular ions needs to prepare ions before the study process. In the conventional methods to get molecular ions, such as electron impact or plasma discharge, a high degree of rotational and vibrational excitation of the prepared molecular ions, even several species of ions, cannot be avoided. The sophisticated method to get molecular ions with state selected has been developed since 1970's. Besides the photoelectron-photoion coincidences (PEPICO) [6], which have been most successfully used to select vibronic states of ions produced by photo-ionization, the powerful method to produce state selected ions is the resonance-enhanced multiphoton ionization (REMPI) with lasers. With REMPI method it is possible to prepare ions with a few (or even one) vibronic states.

The basic principle of REMPI to prepare molecular ions is to excite an intermediate state of the neutral by one or more photons from a pulsed laser and then absorb one or more photons to ionize the excited state. If the last photon is absorbed by a Rydberg state before ionization, it is then possible to produce state selected ions. That is, the first absorbed photon(s)

[a]e-mail: lmzha@ustc.edu.cn; [b]e-mail: slliu@ustc.edu.cn

populate(s) a rovibrational level of a pure neutral Rydberg state converging to an ionic state with a similar geometry, because the removal of a Rydberg electron has little effect on the ion core. The last photon ionizes the Rydberg state following a $\Delta\upsilon = 0$ selection rule, as direct photoionization is governed by Franck-Condon factors [7]. This technique has some unique capabilities: very good resolution allowing one to study rotational energy effects (and possibly alignment); good time and translational energy resolution owing to the short pulses of the lasers (this is very important for dynamics studies); etc [8].

To prepare the molecular ions with state selected by using the photoionization, the basic problem is to excite a Rydberg state of the neutral by one or more photons from a pulsed laser. The search for a suitable ionization pathway of the molecules to be studied requires a detailed knowledge of its optical and photo-ionization spectroscopy. The multiphoton ionization - photoelectron (MPI-PE) spectra of molecules are particularly useful to this kind of study. The MPI-PE spectra of neutral molecule can give not only the suitable REMPI wavelength for the ionization via a Rydberg state, but also the detailed vibrational level population of molecular ions by photoelectron spectra under this REMPI wavelength.

In principle this method produces a single rovibrational ion state. In practice, it is not always the case to get clean state selectivity straightforwardly for two main reasons [7]. Firstly, Rydberg states are seldom pure and are often mixed with other states such as valence states; secondly, multophoton ionization experiments require high laser intensities, this may introduce several ionization paths of molecules to produce the parent molecular ion and the fragment ions simultaneously. Therefore, the key in such experiment is to look for the "soft" multiphoton ionization path of molecules in which mainly the parent molecular ion and only a few fragment ions are formed.

### I-2. The PHOFEX spectrum of molecular ions

To learn the predissociation mechanism of molecular ions, the photofragment excitation (PHOFEX) spectrum of molecular ions is very useful. That is, using a tunable laser to excite the molecular ions to an excited state by one or multi photons, if this excited states cross with a repulsive state then the dissociation of parent ions will occur to produce the fragment ions. By measure the fragment ions yields with the changing of dissociation laser wavelength, the energy level structure and the predissociation information of the excited states of molecular ions could be deduced. Generally speaking, the photofragment excitation spectrum of molecular ions is more convenient in comparing with that of the neutral molecules where the neutral fragment cannot be detected directly by mass methods.

## II. Experiment

The experimental setup [9] consists of (i) a pulsed molecular beam source to generate the jet-cooled $XY_2$ ($XY_2$= $CS_2$, $SO_2$, $N_2O$) molecules, (ii) two dye laser systems pumped independently by two Nd:yttrium–aluminum–garnet (YAG) lasers, and (iii) A home-made time-of-flight (TOF) mass spectrometer.

The jet-cooled $XY_2$ molecules were produced by the supersonic expansion of a $XY_2$/He gas mixture ($XY_2$/He~5-20%) through a pulsed nozzle (General Valve) with a nozzle orifice diameter of 0.5 mm into a photoionization chamber. The laser-molecule interaction region was located 6cm downstream from the nozzle orifice. The time-of-flight mass spectrometer was pumped by two turbomolecular pumps of 500 l/s and 450 l/s. The stagnation pressure was kept at around 1-3 atms, and the operating pressures in the interaction region was $2\times10^{-5}$ Torr.

Two pulsed dye lasers, which were pumped independently by the THG (355 nm) or SHG (532 nm) outputs of two Nd:YAG lasers, were employed in this experiment. The output of one dye laser, 2~5 mJ/pulse, was used as the light source to prepare $XY_2^+$ molecular ions via [3+1] REMPI of $XY_2$ molecules. This photo-ionization laser was focused perpendicularly on the molecular beam of $XY_2$ by a quartz lens with $f$=300 mm or so, and its wavelength was fixed at the three-photon resonance transition of $XY_2$ (483.2 nm for $CS_2$ or 380.2nm for $SO_2$, 360.55 nm for $N_2O$, respectively). The output of another dye laser, 1~3 mJ/pulse, was employed as the photodissociation light to dissociate $XY_2^+$ ions. This light was coaxially counterpropagated with the photoionization laser, and focused by another quartz lens with $f$ =600 mm. Its wavelength was scanned to excite the $XY_2^+$ ions from the ground state to the interest energy region through one- or two-photon excitation. Both dye lasers were temporally and spatially overlapped with each other at the laser-molecule interaction region.

The produced ions, including the parent $XY_2^+$ ions and the fragment ions, were extracted and accelerated into a TOF mass spectrometer and drifted along a TOF tube, and finally detected by a microchannel plate

(MCP) detector. The signals from the MCP output were amplified with a preamplifier, and the mass-resolved data were collected by averaging the amplified signals for selected mass species with boxcar averagers (Stanford SR250), and interfaced to a PC for data storage. The intensities of the ionization laser and the photodissociation laser were monitored simultaneously during the experiment.

## III. The preparation and the dissociation of molecular ions

With the aid of the REMPI spectrum and the available MPI-PE spectrum, we have found the wavelengths for the soft ionization of $CS_2$, $SO_2$, and $N_2O$.

For $CS_2$, we can achieve the soft ionization using the ionization scheme of [3+1] REMPI of $CS_2$ at the wavelength of 483.2 nm. That is, with the ionization laser wavelength at $\lambda_1$=483.2 nm, we could certainly prepare exclusive $CS_2^+$ ions in the $\tilde{X}\,^2\Pi_g$ state with a minimum amount of $S^+$ and $CS^+$ ions [9], using a lens with a middle focus length of $f$ =150 mm and optimizing the pulse energy of the ionization laser at ~1.5 mJ. This process can be expressed as [10],

$$CS_2(\tilde{X}\,^1\Sigma_g^+) \xrightarrow{3h\nu} CS_2(4p\,\sigma\,^3\Pi_u) \xrightarrow{h\nu} CS_2^+(\tilde{X}\,^2\Pi_g)+e,$$

where 4p $\sigma\,^3\Pi_u$ represents for the state of $CS_2$ with a Rydberg orbital of $4p\sigma$.

For $SO_2$, the [3+1] REMPI resonance band located at $\lambda$=380.85 nm can be used to prepare the molecular ion of $SO_2^+(\tilde{X}\,^2A_1)$ via the soft ionization of neutral [11]. That is, the dominating parent ion $SO_2^+$ and very few fragment ions $SO^+$ and $S^+$ can be produced at this wavelength. The amounts of $SO^+$ and $S^+$ ions were less than 1/15 of $SO_2^+$ in our experiment. The [3+1] REMPI of $SO_2$ at $\lambda_1$=380.85 nm can be expressed as

$$SO_2(\tilde{X}\,^1A_1) \xrightarrow{3h\nu_1} SO_2(4pa_1\tilde{G}\,(000)) \xrightarrow{h\nu_1} SO_2^+(\tilde{X}\,^2A_1)+e,$$

where $4pa_1\tilde{G}$ represents for the $\tilde{G}$ state of $SO_2$ with a Rydberg orbital of $4pa_1$. The $\tilde{G}$ Rydberg state with the $A_1$ symmetry converges to the $SO_2^+$ ground state ($\tilde{X}\,^2A_1$) [11]. Though the 13.00 eV energy of four photon with $\lambda_1$=380.85 nm can excited $SO_2$ ($\tilde{X}\,^1A_1$) to a position just above $SO_2^+$ ($\tilde{A}\,^2A_2$) at 12.99 eV, the population of $SO_2^+$ ($\tilde{A}\,^2A_2$) can be omitted, at least, owing to the unfavorable transition of $SO_2^+$ ($\tilde{A}\,^2A_2$) $\leftarrow SO_2$ ($\tilde{G}\,A_1$).

For $N_2O$, the [3+1] REMPI resonance band located at $\lambda$=360.55 nm can be used to prepare the molecular ion of $N_2O^+$ at the ground state $\tilde{X}\,^2\Pi$ via soft ionization of neutral. The [3+1] REMPI at this wavelength of 360.55 nm can be expressed as [12,13]

$$N_2O\,(X^1\Sigma^+) \xrightarrow{3h\nu} N_2O\,(3p\,\sigma\,^1\Pi) \xrightarrow{h\nu} N_2O^+\,(X^2\Pi)+e,$$

where $3p\,\sigma\,^1\Pi$ represents for the excited state of $N_2O$ with a Rydberg orbital of $3p\,\sigma$.

With the elimination of any obvious interference from the background ions, the photodissociation mechanism of the $XY_2^+$ ions can be investigated by introducing the photodissociation laser. By carefully controlling the intensity of the dissociation laser, no ion signal could be observed only with this laser in the scanning wavelength range. Remarkably strong signal of fragment ion appeared in TOF mass spectrum with both lasers. The fragment ions were confirmed to be generated completely from the interaction of the dissociation laser on the parent molecular $XY_2^+$ ions, by varying the temporal delay and the spatial overlap between the two lasers. To avoid interference from the autoionization of neutral $XY_2$, there was an ~60 ns delay temporally and a slight separation in the direction of ion flight between the dissociation laser and the ionization laser in the laser-molecule interaction region. As an example, it is shown in Figure 1 that a remarkably strong $S^+$ fragment ion signal appears in TOF mass spectrum (c) with both the ionization laser and the dissociation laser matched spatially and temporally with each other, but the parent molecular $CS_2^+$ ions are dominated (a) only with ionization laser acting.

## IV. PHOFEX Spectrum and [1+1] Photodissociation Mechanism for $CS_2^+$ [9,14].

### IV-1. PHOFEX Spectrum of $CS_2^+$

In addition to the three bound electronic states of $\tilde{X}$, $\tilde{A}$, $\tilde{B}$ of $CS_2^+$ [15,16], the higher excited state, named as $\tilde{C}\,^2\Sigma_g^+$, was observed from the photoelectron spectroscopy [17–19] and studied further by Frey *et al.* [20] and Wang *et al.* [21] to determine the vibrational frequencies. The $\tilde{C}\,^2\Sigma_g^+$ state was determined to be fully predissociative and correlated with both $S^+$+CS and S+$CS^+$ fragments [22]. The dissociation dynamics in the $\tilde{C}\,^2\Sigma_g^+$ state was studied in detail by Maier and co-workers [23,24] and recently by Hwang *et al* [25]. In both of their studies, the method of two-color optical–optical double resonance transitions of $CS_2^+(\tilde{C}\,^2\Sigma_g^+) \leftarrow CS_2^+(\tilde{B}\,^2\Sigma_u^+) \leftarrow CS_2^+(\tilde{X}\,^2\Pi_g)$ with the mass selected was used. Although it was proposed that [26] the curve crossing from the $\tilde{C}\,^2\Sigma_g^+$ state to a fully repulsive $^4\Sigma^-$ or/and a repulsive $^2\Sigma^-$ state should be responsible for the

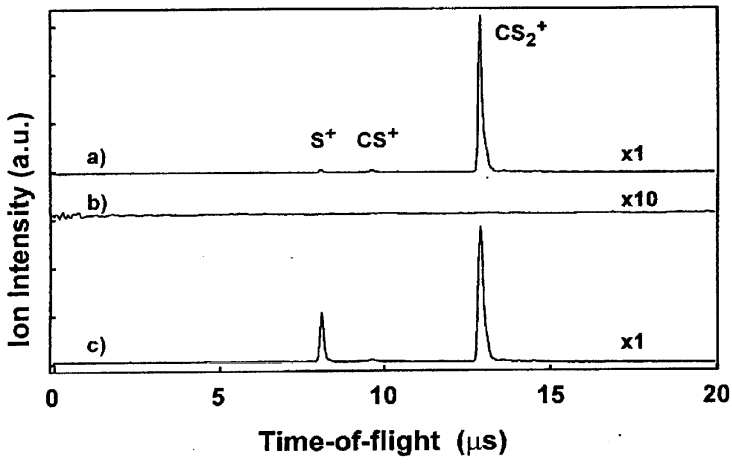


**Figure 1:** The TOF mass spectra averaged over 256 laser shots and obtained with (a) only the photoionization laser at 483.2 nm, (b) only the photodissociation laser at 460.6 nm and (c) both the photoionization laser and the dissociation laser overlapped spatially and temporally with each other. The $CS_2^+$ ions in (a) and (c) were generated via [3+1] REMPI of $CS_2$ molecules by the ionization laser, and the $S^+$ ions in (c) were produced from the dissociation of $CS_2^+$ ions by the dissociation laser. The pulse energies of the ionization laser and the dissociation laser were optimized and maintained at 2 and 1 mJ, respectively.

predissociation in $CS_2^+$ that lead to $S^+(^4S)$+$CS(X\,^1\Sigma^+)$ and $CS^+(X\,^2\Sigma)$+$S(^3P)$, the following questions concerning the dissociation in $CS_2^+$ still remain to be answered: (i) is the predissociation in $CS_2^+$ that lead to $CS^+(X\,^2\Sigma)$ +$S(^3P)$ required to occur via the $\tilde{C}\,^2\Sigma_g^+$ state? and (ii) where is the adiabatic appearance potential to the second dissociation limit $CS^+(X\,^2\Sigma)$+$S(^3P)$ of $CS_2^+$. The following PHOFEX spectrum will be used to answer these questions.

In the wavelength range of 385-482 nm the one-photon excitation energy can access neither the first dissociation limit $S^+(^4S)$+$CS(X^1\Sigma^+)$ nor the second dissociation limit $CS^+(X\,^2\Sigma^+)$+$S(^3P)$ of the $CS_2^+$ ion from its electronic ground state [26]; therefore, the two-photon excitation of the parent $CS_2^+$ ions by the dissociation laser is needed to produce $S^+$ and $CS^+$ ions. Figure 2 shows the PHOFEX spectrum by monitoring $S^+$ ions in the wavelength range of 385–485 nm [14]. With the aid of the spectroscopic data obtained from previous studies on the spectroscopy of $CS_2^+$ [7,9,14,15,18,32], this PHOFEX spectrum could be assigned completely as the radiative electronic transition $CS_2^+$ $(\tilde{A}\,^2\Pi_u) \leftarrow$ $CS_2^+$ $(\tilde{X}\,^2\Pi_g)$. This observation means that the two-photon excitation of parent $CS_2^+$ ions by dissociation laser is a [1+1] sequent excitation and the intermediate state in the [1+1] dissociation process to generate $S^+$ is the $\tilde{A}\,^2\Pi_u$ state of the $CS_2^+$ ion. As indicated in Figure 2, the observed resonance peaks in the spectrum correspond to transitions from the (0,0,0) vibrational levels [9,14,27] in the $\tilde{X}\,^2\Pi_{g,3/2}$ state to the $\upsilon = 0 - 7$ vibrational levels in the $\tilde{A}\,^2\Pi_{u,3/2}$ state and to transitions from the (0,0,0) vibrational levels in the $\tilde{X}\,^2\Pi_{g,1/2}$ states to the $\upsilon = 0 - 3$ vibrational levels in the $\tilde{A}\,^2\Pi_{u,1/2}$ states, where $\upsilon$ represents a group of vibrational levels coupled through Fermi resonance interaction and is defined as $\upsilon = \upsilon_1 + (\upsilon_2/2)$ (here, $\upsilon_1$ and $\upsilon_2$ denote vibrational quantum numbers for the $\nu_1$ (symmetric stretch) and $\nu_2$ (bend) modes, respectively). Interestingly, Figure 2 shows that the intensities of the transition progression of $\tilde{A}\,^2\Pi_{u,1/2}(\upsilon_1, \upsilon_2, 0) \leftarrow \tilde{X}\,^2\Pi_{g,1/2}(0,0,0)$ is much weaker than that of $\tilde{A}\,^2\Pi_{u,3/2}(0,0,0) \leftarrow \tilde{X}\,^2\Pi_{g,3/2}(0,0,0)$. This can be explained, at least, by the strong population of $\tilde{X}\,^2\Pi_{g,3/2}(0,0,0)$ and

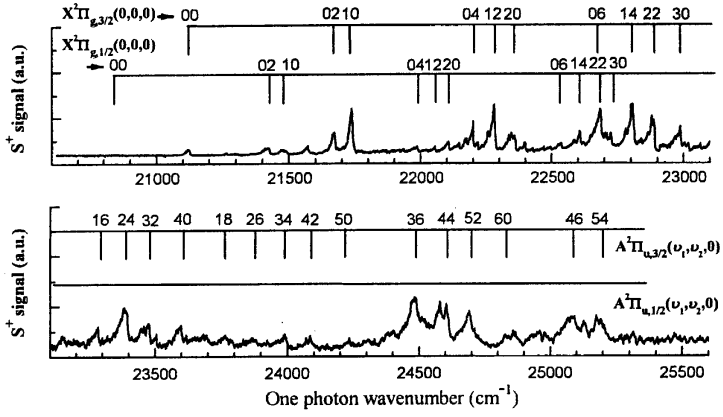


**Figure 2:** PHOFEX spectrum obtained by monitoring $S^+$ ions in the wavelength range of 385-485 nm. The spectrum was assigned to two series of $\tilde{A}^2\Pi_{u,3/2}(\upsilon_1, \upsilon_2,0) \leftarrow \tilde{X}^2\Pi_{g,3/2}(0,0,0)$ and $\tilde{A}^2\Pi_{u,1/2}(\upsilon_1, \upsilon_2,0) \leftarrow \tilde{X}^2\Pi_{g,1/2}(0,0,0)$ vibronic transitions of the $CS_2^+$ ion, indicating that the $S^+$ ions were generated from the $\tilde{A}$ state-intermediated two-photon dissociation process of the $CS_2^+$ parent ions by the dissociation laser. The spectrum was not corrected for the laser energy.

the weak population of $\tilde{X}^2\Pi_{g,1/2}(0,0,0)$ with the [3+1] REMPI of the $CS_2$ at the ionization laser wavelength of $\lambda_1$=483.2 nm [27].

### IV-2. Adiabatic Appearance Potential (AP) of $CS^+$

In Figure 3, the $S^+$ and $CS^+$ PHOFEX spectra obtained by monitoring the $S^+$ and $CS^+$ species simultaneously were given in the range of 46000-51600 $cm^{-1}$ (two-photon energy). It is shown that the yield of $CS^+$ ion obviously increases at a two photon energy position of ~47200 $cm^{-1}$. The $CS^+$ PHOFEX spectrum, in comparing to the $S^+$ PHOFEX spectrum, has a similar spectral structure, within the wavenumber range of 47388-51000 $cm^{-1}$. Around the appearance position of the $CS^+$ ion there is a remarkable resonance band that was assigned to the one photon transition of $\tilde{A}^2\Pi_{u,3/2}(4,0,0) \leftarrow \tilde{X}^2\Pi_{g,3/2}(0,0,0)$; therefore it is reasonable to determine the AP value of the $CS^+$ ion as 47196±40 $cm^{-1}$ above the $CS_2^+(\tilde{X}^2\Pi_{g,3/2}(0,0,0))$ level, as shown in Figure 3. Obviously, this method to excite the $CS_2^+$ parent ion directly can give a more precise and reliable value of $CS^+$ adiabatic appearance potential (that is 5.852±0.005 eV above the $CS_2^+(\tilde{X}^2\Pi_{g,3/2}(0,0,0))$ level, or 15.930±0.005 eV above the $CS_2(X^1\Sigma_g^+(000))$ level).

### IV-3. [1+1] Photodissociation Mechanism

Note that the $CS^+$ appearance potential of 47196 $cm^{-1}$ is lower than the energy position of the $CS_2^+(\tilde{C}^2\Sigma_g^+(000))$ level at 49282 $cm^{-1}$ [23], as shown in Figure 3. That is, in the energy range of the photodissociation laser (<6.11/2 eV), the [1+1] two-photon excitation cannot energetically reach the $\tilde{C}^2\Sigma_g^+$ state but can reach the energy region of high vibrational levels in the $\tilde{B}^2\Sigma_u^+$ state. This observation means that the appearance of the $CS^+$ ion does not need to proceed via the $CS_2^+(\tilde{C}^2\Sigma_g^+)$ level and follow coupling between the $\tilde{C}$ electronic state and the $^4\Sigma^-$ or/and $^2\Sigma^-$ repulsive state. To produce $CS^+$ via $^4\Sigma^-$ repulsive state in this energy region, the photoexcitation to $\tilde{B}^2\Sigma_u^+$ state and the couple between the $\tilde{B}^2\Sigma_u^+$ state and the $^4\Sigma^-$ repulsive state are needed. Obviously, an electronic transition of the $CS_2^+$ ion from the $\tilde{A}^2\Pi_u$ state to the linear excited state $\tilde{B}^2\Sigma_u^+$ is strongly forbidden in a one-photon excitation by the electric dipole selection rule. Therefore, the intensity in this forbidden $\tilde{B}^2\Sigma_u^+ \leftarrow \tilde{A}^2\Pi_u$ transition, if it exist, should come from the vibronic coupling of $\tilde{A}^2\Pi_u$ and $(\tilde{X}^2\Pi_g)^\dagger$, where "the dagger symbol † represents high vibrational levels in the corresponding electronic states. Note that in the first step of excitation of the $CS_2^+$ ion, it is not necessary to

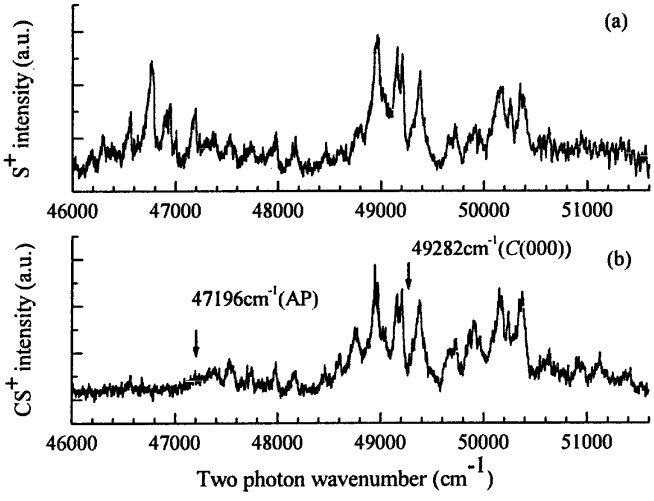


**Figure 3:** PHOFEX spectra obtained by monitoring (a) $S^+$ ions and (b) $CS^+$ ions in the range of 46000-51600 $cm^{-1}$ (two photon energy). The two arrows in panel (b) indicate the position of the appearance potential (AP) of the $CS^+$ ion (at 47196 $cm^{-1}$) and that of the $\tilde{C}(000)$ level of the $CS_2^+$ ion (at 49282 $cm^{-1}$).

call for a complete relaxation to the $(\tilde{X}\,^2\Pi_g)^\dagger$ followed by excitation to $\tilde{B}\,^2\Sigma_u^+$, because only the g→u→u sequence of the electronic inversion symmetries is needed to the transitions of $\tilde{X}\,^2\Pi_g \rightarrow \tilde{A}\,^2\Pi_u \rightarrow \tilde{B}\,^2\Sigma_u^+$. That is, the vibronic inversion symmetry that characterizes the $\tilde{A}^2\Pi_u \rightarrow (\tilde{X}\,^2\Pi_g)^\dagger$ coupling (u) will be conserved, regardless of the state they say the second step originates from. The final state must be vibronically g for the transition matrix element to be nonzero. This can only occur for a $\tilde{B}\,^2\Sigma_u^+$ final state if the overall transition from the original level in $\tilde{X}\,^2\Pi_g$ is accompanied by an odd change in the bend or asymmetric stretch quantum number. According to the vibronic coupling theory [29] for a linear triatomic molecules of $D_{\infty h}$ symmetry, such as $CS_2^+$, with the $\nu_1$ ($\Sigma_g^+$) symmetric stretching vibration, $\nu_2$ ($\Pi_u$) bending vibration and $\nu_3$ ($\Sigma_u^+$) asymmetric stretching vibration, it could happen that one excites from the $\tilde{X}\,^2\Pi_g$ (0,0,0) level to the $\tilde{A}\,^2\Pi_u$ ($\upsilon_1$, 2m, 2n) level and that this state couples resonantly with ($\tilde{X}\,^2\Pi_g$ ($\upsilon_1$', 2m'+1, 2n') )$^\dagger$, where m, n, m', n'=0, 1, 2, ... These states both have u (most probably $\Pi_u$ Renner) vibronic symmetry and can be simply regarded as a mixed state. Now to excite to the $\tilde{B}\,^2\Sigma_u^+$ state, the only transitions allowed are those that terminate on an odd-numbered bending level (which could be viewed as vertical in a sense or an even change from the coupled $\tilde{X}^\dagger$ component and different by an odd number from A; however, this distinction is unnecessary and is, in effect, lost in the vibronic interaction). A similar logic applies to transitions and coupling facilitated by excitation in an asymmetric stretch; that is, the $\tilde{A}\,^2\Pi_u$ ($\upsilon_1$, 2m, 2n) level couples resonantly with the ($\tilde{X}\,^2\Pi_g$ ($\upsilon_1$', 2m', 2n'+1))$^\dagger$, where m, n, m', n'=0, 1, 2,... These states also both have u vibronic symmetry and can be simply regarded as a mixed state. Moreover, the coupling of the $\tilde{B}\,^2\Sigma_u^+$ state and the $^2\Sigma^-$ repulsive state, which lies a little higher than the $^4\Sigma^-$ repulsive state, in regard to energy, should also give its contribution to the $CS^+$ fragmentation process of the $CS_2^+$ ion in the shorter wavelength. The $S^+$ fragmentation of the $CS_2^+$ ion, with a lower appearance potential than that of $CS^+$, has the similar [1+1] photodissociation mechanism.

The proposed dynamics for the [1+1] photodissociation process of $CS_2^+$ to produce the $S^+$ and $CS^+$ fragment ion can be summarized as follows: (i) the

$CS_2^+$ ($\tilde{A}\,^2\Pi_u$) ← $CS_2^+$($\tilde{X}\,^2\Pi_g$) transition through one-photon excitation, (ii) $CS_2^+$ ($\tilde{A}\,^2\Pi_u$) → $CS_2^+$ ($\tilde{X}^\dagger$) via an internal conversion process (because of the vibronic coupling between the $\tilde{A}$ state and the $\tilde{X}$ state by the $\nu_2$ ($\Pi_u$) bending vibration or the $\nu_3$ ($\Sigma_u^+$) stretching vibration), (iii) $CS_2^+$ ($\tilde{X}^\dagger$) → $CS_2^+$ ($\tilde{B}\,^2\Sigma_u^+$) through the second photon excitation, and (iv) $CS_2^+$ ($\tilde{B}\,^2\Sigma_u^+$) → $CS^+(X^2\Sigma^+)$+S($^3$P) or/and $CS_2^+$($\tilde{B}\,^2\Sigma_u^+$) → $S^+(^4S)$+CS($X^1\Sigma^+$), because the energy curve crossing with the repulsive $^4\Sigma^-$ state and/or $^2\Sigma^-$ state correlated with the second dissociation limit.

It can be deduced from the data of Figure 3 that the branching ratio of $CS^+/S^+$ increases from 0 at 47200 $cm^{-1}$ to slightly larger than 1 at ~50400$cm^{-1}$ [14]. This result is not only similar in energy to that measured at the $\tilde{C}$ state by Hwang *et al.* [25], but also is agreement with that given in the PEPICO experiment conducted by Aitchson and Eland [37]. Further detailed data on the electronic states of $CS_2^+$ is needed to explain that the dissociation probability to $CS^+$+S increases as the two-photon potential of the dissociation laser increased, as shown by the branching ratio of $CS^+/S^+$.

Figure 4 schematically shows the relevant potential levels of the $CS_2^+$ ion modified from Refs. 23, 26, and 28, as well as the possible interactions among the electric states in the [1+1] excitation and dissociation process to $CS^+$+S.

## V. PHOFEX spectrum and the predissociation mechanism for $SO_2^+$ [30,31]

### V-1. Photofragment $SO^+$ excitation spectrum

The photoelectron spectroscopy with molecular beam [32,33], and the photoionization [34,35] of $SO_2$ molecule have been used to provide the vibration structure for the electronic states of $SO_2^+$ including the overlapped $\tilde{E},\tilde{D},\tilde{C}$ states. The common ground of above methods is to excite the neutral molecule $SO_2$ by using high energy photons. The available photodissociation spectrum of $SO_2^+$ ion by the direct photoexcitation of $SO_2^+$ itself is from Thomas *et al* [36]. In their study, the $SO_2^+$ ions prepared by electron impact were selected by a triple quadrupole system and the photodissociation spectrum of $SO_2^+$ ion was obtained by the coaxial irradiation of tunable dye laser. However, the signal-noise ratio and resolution for their photodissociation spectra of $SO_2^+$ ion seem poor.

Figure 5 shows the PHOFEX spectrum obtained in the wavelength range of 291-312 nm with the ionization laser fixed at 380.85 nm. In the entire scan range the signal of $SO^+$ ion is dominated comparing to the very weak $S^+$ ion signal. The obvious resonance bands are shown in the PHOFEX spectrum by measuring $SO^+$. According to the spectroscopic data obtained from previous studies on the photoelectron

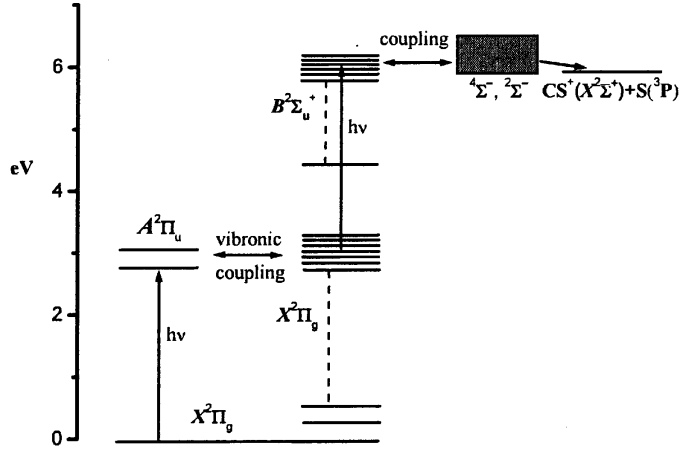


**Figure 4:** Schematic energy level diagram of the $CS_2^+$ ion with possible interactions among the electronic states, to illustrate the [1+1] excitation and dissociation process.

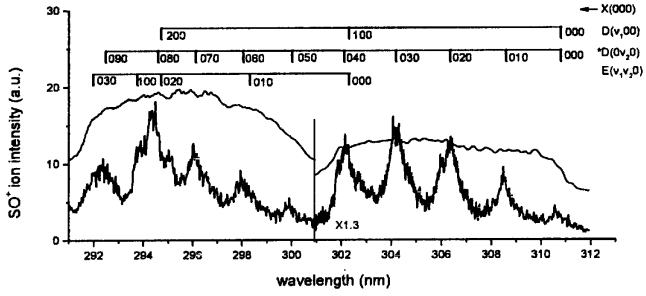


**Figure 5:** The PHOFEX spectrum of $SO_2^+$ obtained by monitoring $SO^+$ ions in the wavelength range of 291-312 nm. The new bend vibration series is marked by "*". The spectrum was assigned with the aid of photoelectron spectrum in Refs. 26 and 33. No correction is made to the laser efficiency. The laser efficiency curve was given at the top of spectra in figure.

spectroscopy of $SO_2$ [32,33], the one photon energy in the wavelength range of 291-312 nm can excite the allowed transitions of $SO_2^+(\tilde{E},\tilde{D},\tilde{C}) \leftarrow SO_2^+(\tilde{X}\,^2A_1)$ [41], where $\tilde{E},\tilde{D},\tilde{C}$ posses one kind of $^2B_2$, $^2B_1$, and $^2A_1$ symmetry, respectively. It is found that if only to assign the PHOFEX spectrum to the transitions from the vibration level (000) of $SO_2^+$ ($\tilde{X}\,^2A_1$) the complete vibration series could be obtained for the PHOFEX spectrum, as shown in Figure 5. This means that in the [3+1] REMPI of $SO_2$ the excited $SO_2(4pa_1\,\tilde{G}\,(000))$ converges to $SO_2^+$ ($\tilde{X}\,^2A_1$ (000)) finally.

The assignments of $\tilde{D}(\upsilon_1$=0-2, $\upsilon_2$=0, $\upsilon_3$=0) $\leftarrow \tilde{X}\,^2A_1$ (000) and $\tilde{E}(\upsilon_1$=0, 1, $\upsilon_2$=0-3, $\upsilon_3$=0)) $\leftarrow \tilde{X}\,^2A_1$ (000) of $SO_2^+$ were deduced from the data of photoelectron spectra [33] and was shown in Figure 5. To assign other resonance bands in PHOFEX spectrum we first try to assign them to $SO_2^+$ ($\tilde{C}$)$\leftarrow SO_2^+(\tilde{X}\,^2A_1)$ transition. However, it is failed to found the series of $SO_2^+$ ($\tilde{C}$) $\leftarrow SO_2^+(\tilde{X}\,^2A_1(000))$ transition in the PHOFEX spectrum of 291-312 nm as well as in the much weaker PHOFEX spectrum of 312-332 nm, although the allowed transitions of $SO_2^+(\tilde{C}) \leftarrow SO_2^+(\tilde{X}\,^2A_1(000))$ predicted by the newly PES spectrum [32,33] should locate in this wavelength range.

It is very interesting that the three resonance bands with the adjacent space of ~230 $cm^{-1}$, located at 304.20, 306.36, and 308.60 nm, respectively, cannot be assigned reasonably by using the available spectral data of $SO_2^+$ [32,33] as mentioned above. Owing to the energy positions of these bands being between $SO_2^+$ ($\tilde{D}$(000)) and $SO_2^+$ ($\tilde{E}$(000)), it is reasonable to assign these bands to the transitions of $\tilde{D}(0\ \upsilon_2\ 0) \leftarrow \tilde{X}\,^2A_1$ (000) for $SO_2^+$, where $\upsilon_2$ is the bend vibration quantum numbers. The important supporting for this assignment is the large change of molecular bond angle from 136.5° of $SO_2^+$ ($\tilde{X}\,^2A_1$) to 119.5° of $SO_2^+$ ($\tilde{D}$), which is favorable to excite the transition to the bent vibration levels of $SO_2^+$ ($\tilde{D}$) from $SO_2^+$ ($\tilde{X}\,^2A_1$). The bend vibration excitation of $SO_2^+$ ($\tilde{D}$) was not given in photoelectron spectrum [32,33], maybe owing to the nearly same molecular bond angle of 119.5° for $SO_2^+(\tilde{D})$ and $SO_2(\tilde{X}\,^1A_1)$ [37], which is unfavorable to excite the bent vibration mode of $SO_2^+(\tilde{D})$ from $SO_2(\tilde{X}\,^1A_1)$. Following this assignment, the bend vibration levels from $\upsilon_2$=0 to $\upsilon_2$=9 of $SO_2^+$ ($\tilde{D}(0\ \upsilon_2\ 0)$ was obtained, as shown in Figure 5. New harmonic bend vibrational frequency $\nu_2$=241.8 ±0.9 $cm^{-1}$ and the anharmoniccity constants $X_{22}$= −1.7 ±0.1 $cm^{-1}$ for $SO_2^+$ ($\tilde{D}$) were deduced by using least-squares fitting. The lower $\nu_2$ of ~240 $cm^{-1}$ for $\tilde{D}$ state, given by us, in comparison with $\nu_2$ of ~360 $cm^{-1}$ for the $\tilde{C}$ state, given by the photoelectron spectrum, means that the potential curve of $\tilde{D}$ state is not similar to other states along the bend vibrational coordinate, further studies both in experiment and in theory are needed. It is worth to

notice that the rotational structure of resonance bands in PHOFEX spectrum cannot be resolved even with a spectral resolution of ~0.1 $cm^{-1}$ from dissociation laser. The broader shape of resonance band, such as at 306.36 nm, may be from the distribution of rotational transition and the further study is needed.

### V-2. The symmetry and the predissociation mechanism of $SO_2^+$ ($\tilde{D}$)

Although the photoelectron-photoion coincidence (PEPICO) spectroscopy has been used to investigate the unimolecular dissociation of $SO_2^+$ ($\tilde{C},\tilde{D},\tilde{E}$) excited from the neutral $SO_2$ [38-40], the direct excitation of molecular ions using laser is more convenient to study the predissociation mechanism of $SO_2^+$ ($\tilde{C},\tilde{D},\tilde{E}$). To learn the predissociation process of $SO_2^+$ ($\tilde{D}$) two photon transitions of $SO_2^+$ ($\tilde{X}\,^2A_1$) in the range of 562-668 nm, by which the energy position of $SO_2^+$ ($\tilde{D}$) can be reached, were completed. It is interesting that the continuous PHOFEX spectrum without discernible band structure in this visible range was obtained by measuring $SO^+$. The obvious difference between the PHOFEX spectrum in UV range and that in visible range can be explained as follows. For the molecule with $C_{2v}$ point group symmetry, like $SO_2^+$, the transition of $^2B_1$, $^2A_1$, $^2B_2 \leftarrow \tilde{X}\,^2A_1$ are allowed, but the transition of $^2A_2 \leftarrow \tilde{X}\,^2A_1$ is forbidden [20] for one photon excitation. However, the transitions both of $^2B_1$, $^2A_1$, $^2B_2 \leftarrow \tilde{X}\,^2A_1$ and of $^2A_2 \leftarrow \tilde{X}\,^2A_1$ are allowed for two photon excitation. Notice that the energy position, reached either by one photon excitation of 283-332 nm laser or by two photon excitation of 562-664 nm laser, should be the same, when $SO_2^+$ ($\tilde{X}\,^2A_1$) was excited. Thus, the similar PHOFEX spectrum should be obtained by using 281-332 nm laser or by using 562-664 nm laser, if there is only $^2B_1$, $^2A_1$, $^2B_2 \leftarrow \tilde{X}\,^2A_1$ transitions. However, the obvious resonance band structure appeared in the PHOFEX spectrum of 281-332 nm and the continuum appeared in the PHOFEX spectrum of 562-664 nm. This fact can be explained if there is a repulsive state of $^2A_2$ symmetry around $\tilde{D}$ states, which is allowed for two-photon excitation and is forbidden for one photon excitation from $\tilde{X}\,^2A_1$. We call this supposed repulsive state as $\alpha^2A_2$. Although the two photon transition in the range of 562-664 nm could excite $SO_2^+$ ($\tilde{X}\,^2A_1$) into the $^2B_1$, $^2A_1$, $^2B_2$ states correlated to $\tilde{E},\tilde{D},\tilde{C}$, the direct dissociation rate via $\alpha^2A_2$ repulsive state excited by two photon transition will be much larger than the predissociation rate via $^2B_1$, $^2A_1$, $^2B_2$ states correlated to $\tilde{E},\tilde{D},\tilde{C}$ [34], and the total effect will be like the direct dissociation. Thus, it is not surprising that only the continuous PHOFEX spectrum without discernible resonance band structure was obtained by using two photon transition in the range of 562-664 nm. Notice that if the "pure" two photon transition in the range of 562-664 nm is replaced by [1+1] transition via the congested vibration levels of the $\tilde{B}\,^2B_2$ state [32,33], the above-presented discussion is still effective.

The symmetry of $\tilde{E},\tilde{D},\tilde{C}$ is still an arguable problem, although they were denoted as $\tilde{E}\,^2B_1,\tilde{D}\,^2A_1,\tilde{C}\,^2B_2$, respectively, in several references [32-34]. For example, according to the calculated results of *Ab initio* SCFMO by Hillier and Saunders [37], the three electronic states located at 16.50, 16.34 and 15.90 eV, respectively, should be denoted as $\tilde{E}\,^2B_2,\tilde{D}\,^2A_1,\tilde{C}\,^2B_1$. Thomas *et al.* [36] questioned the assignment of $\tilde{D}\,^2A_1$, and proposed the assignment of $\tilde{D}\,^2B_2$ and the possible assignment of $\tilde{C}\,^2B_1$.

To explain the PHOFEX spectra of $SO_2^+$ in UV range, the predissociation mechanism of $\tilde{D}$ bound state need to be considered. Owing to the fact that the $\tilde{D}$ state belongs to one of the $^2B_1$, $^2A_1$, $^2B_2$ bound states, it could not couple to the $\alpha^2A_2$ repulsive state by electron-electron interaction, but the coupling by electron-vibration interaction between $\tilde{D}$ state and $\alpha^2A_2$ repulsive state is possible. $SO_2^+$ is a triple atomic planar molecule ion with $C_{2v}$ point group symmetry, $C_2(z)$, and the molecular axis along the y coordinate in the molecular plane. The possible vibrational mode could be that of $a_1$ and $b_2$ symmetry and the impossible vibration modes are that of $b_1$ and $a_2$ symmetry which need change symbol for the nucleus reverse about molecular plane [41]. If the direct product of $\tilde{D}$ electronic state and vibration $a_1$ and $b_2$ contains $^2A_2$ symmetry, then the coupling between the electronic states among $\tilde{D}$ and the $\alpha^2A_2$ repulsive state via electron vibration interaction is possible. Obviously, only the $\tilde{D}$ state with $^2B_1$ symmetry satisfies the above-mentioned condition ($B_1 \times b_2 = A_2$) and can couple to the $\alpha^2A_2$ repulsive state via electron vibration interaction. Thus, the symmetry of the $\tilde{D}$ state is determined as $^2B_1$ and $\tilde{D}\,^2B_1$ predissociate to $SO^+(X^2\Pi) + O(^3P_g)$ by coupling

to $\alpha^2A_2$ rcpulsive state via electron vibration interaction.

The whole excitation and dissociation processes of $SO_2^+$ in the present study can be expressed as

$SO_2^+(\tilde{X}^2A_1) \xrightarrow{h\nu_2(UV)} SO_2^+(\tilde{D}^2B_1)$,

$SO_2^+(\tilde{D}^2B_1) \xleftarrow{coupling} SO_2^+(\tilde{\alpha}^2A_2)$,

$SO_2^+(\tilde{X}^2A_1) \xrightarrow{2h\nu_2(visible)} SO_2^+(\tilde{\alpha}^2A_2)$,

$SO_2^+(\tilde{\alpha}^2A_2) \rightarrow SO^+(X^2\Pi)+O(^3P_g)$.

## VI. The PHOFEX spectrum and the channel switching effect of $N_2O^+$

### VI-1. The PHOFEX spectrum of $N_2O^+$

Figure 6 shows the $NO^+$ PHOFEX spectrum [42] in the wavelength range of 278–328 nm which has been corrected for the variation of excitation laser intensity. Due to the different experimental technique employed in this work, the present spectrum reveals many new

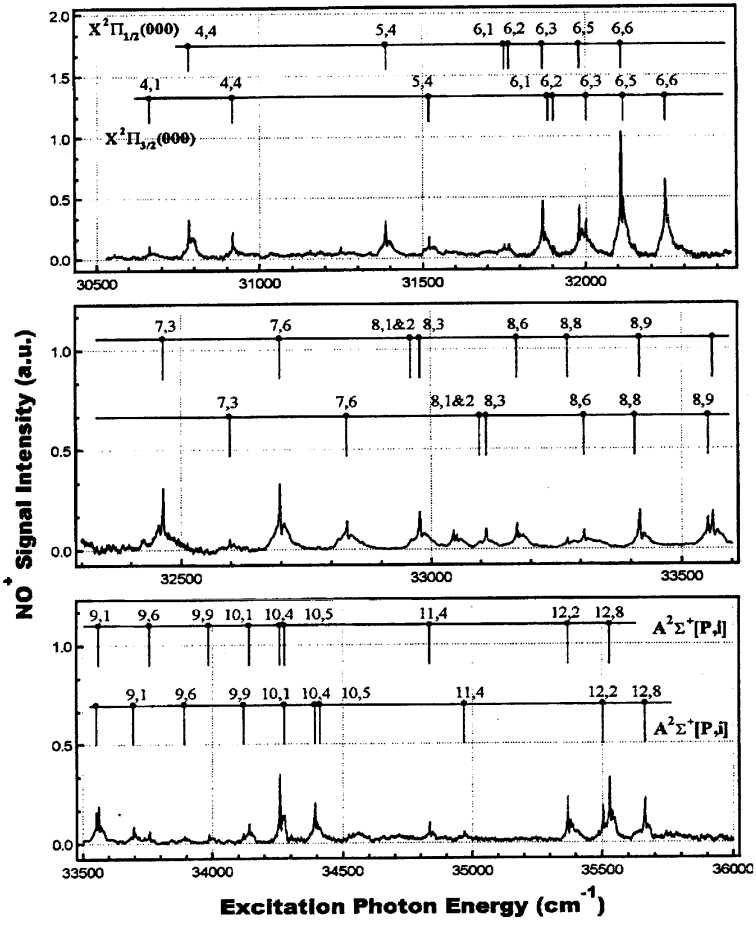


**Figure 6:** The PHOFEX spectrum of $N_2O^+$ obtained by monitoring $NO^+$ fragment in the wavelength range of 275–328 nm, which is attributed to $A^2\Sigma^+ \leftarrow X^2\Pi_{1/2,3/2}(000)$ electronic transition and assigned in terms of Fermi-resonance coupled vibrational levels in the $A\ ^2\Sigma^+$ state. The spectrum consists of many newly observed vibronic bands.

vibronic features, which were not observed in all previous studies regarding the $A\ ^2\Sigma^+$ state of $N_2O^+$, and thus should make our spectral analysis more reliable and provide more detailed spectroscopic information about the $A\ ^2\Sigma^+$ state.

The $A^2\Sigma^+$ state of $N_2O^+$ ions is known to be linear, and has similar geometries to its electronic ground state $X^2\Pi$. The vibrational frequencies $\nu_1$ (symmetry stretching), $\nu_2$ (bending), and $\nu_3$ (anti-symmetric stretching) of $N_2O^+$ ($A^2\Sigma^+$) are known to be around 1346, 611, and 2450 $cm^{-1}$, respectively, as determined from the fluorescence emission study [43], FIBLAS studies [44-49], and photoelectron measurements [50]. Based upon the known vibrational frequencies of $N_2O^+$ ($A^2\Sigma^+$) and several observed $A^2\Sigma^+ \rightarrow X^2\Pi$ (000) vibronic transitions in emission studies, tentative assignments were performed to the PHOFEX spectrum. It was found that except for a few peaks in the low excitation energy region in Fig. 6, most of the transitions could not be assigned properly into excitations of $\nu_1$, $\nu_2$, and $\nu_3$ mode vibrational progressions of the $A^2\Sigma^+$ state or their combinations, even if taking into account of the anharmonic constants.

In fact, since the vibrational frequencies of $N_2O^+$ ($A^2\Sigma^+$) have the approximate relations $\nu_3 \sim 2\ \nu_1 \sim 4\ \nu_2$, Fermi-resonance interaction is expected to occur between the $(V_1,V'_2,V_3)$ and $(V_1\text{-}1,(V_2\text{+}2)',V_3)$, or $(V_1,V'_2,V_3)$ and $(V_1\text{+}2,V'_2,V_3\text{-}1)$ vibrational levels, where $V_1$, $V_2$, $V_3$, and $l$ represent the vibrational quantum numbers of $\nu_1$, $\nu_2$, and $\nu_3$ modes and the vibrational angular momentum, respectively. Therefore, the Fermi interaction makes zero-order vibrational eigenstates mixed with each other, and it is unfeasible to perform the spectral assignment in normal way, especially for transitions to high vibrational levels. As stated by Bernath *et al.* [51], such a coupled cluster of zero-order vibrational levels can be represented by a polyad quantum number P, which is defined as $P=2V_1+V_2+4V_3$ in present case. Then, only vibrational levels with the same $P$ and $l$ interact with each other. Since the zero-order levels in a polyad mix with each other by Fermi interaction, using expression $(V_1, V_2, V_3)$ to label the vibrational level will lose its meaning, we therefore refer to the eigenstates as $[P,i]$, where $i$ represents the energy ordering number within the polyad increasing with the energy.

Due to the Fermi interaction in the $A^2\Sigma^+$ state, the vibrational energy term values have to be obtained by diagonalizing an effective Hamiltonian matrix, rather than by a simple Dunham expansion. If inter-polyad interactions are ignored, the effective Hamiltonian matrix is block diagonalized for each polyad quantum number $P$. The diagonal matrix element, i.e., the zero-order unperturbed vibrational energy, can be expressed by a Dunham expansion as

$$\left\langle V_1,V_2^l,V_3\left|\hat{H}^{eff}\right|V_1,V_2^l,V_3\right\rangle = G(V)$$

$$= \sum_i \nu_i\left(V_i+\frac{d_i}{2}\right) + \sum_{ij}\chi_{ij}\left(V_i+\frac{d_i}{2}\right)\left(V_j+\frac{d_j}{2}\right) + g_{22}l^2, \quad (1)$$

where $\hat{H}^{eff}$ refers to the effective Hamilton, $\chi_{ij}$ and $d_i$ are the anharmonic constant and the degeneracy of vibrational mode, respectively. Since in this experiment only vibrational levels of $A^2\Sigma^+$ state with $l$=0 (for even $P$) or $l$=1 (for odd $P$) can be observed via excitation from the $X^2\Pi(000)$ state, we may omit the small contribution of $l$=1 to the vibrational energy in Eq. (1). The off-diagonal matrix elements for each block are

$$\left\langle V_1,V_2^l,V_3\left|\hat{H}^{eff}\right|V_1+1,(V_2-2)^l,V_3\right\rangle = \frac{1}{2\sqrt{2}}K_{122}\sqrt{(V_2-l)^2(V_1+1)}, \quad (2)$$

$$\left\langle V_1,V_2^l,V_3\left|\hat{H}^{eff}\right|V_1+2,V_2^l,V_3-1\right\rangle = \frac{1}{2\sqrt{2}}K_{133}\sqrt{V_3(V_1+1)(V_1+2)}, \quad (3)$$

where $K_{122}$ and $K_{113}$ represent the constants of Fermi-resonance interactions between $\nu_1$, $\nu_2$ modes and $\nu_1$, $\nu_3$ modes, respectively. Here, we also ignore the higher order Fermi interactions, such as interactions between the $(V_1,V_2,V_3)$ and $(V_1\text{-}2,V_2\text{+}4,V_3)$ levels, $(V_1,V_2,V_3)$ and $(V_1,V_2\text{+}4,V_3\text{-}1)$ levels. Note that within the excitation energy range in this experiment, the $\nu_3$ mode of the $A^2\Sigma^+$ state can only be excited as high as $V_3$=3, the number of vibrational levels involving $\nu_3$ mode are relatively less than those involving $\nu_1$ and $\nu_2$ modes, therefore, we also neglect the interaction between $\nu_1$ and $\nu_3$ modes, i.e., fix $K_{113}$=0.

By diagonalizing the effective Hamilton matrix and fitting the identified transition peaks with a least-square procedure, the PHOFEX spectrum were assigned completely as the $A^2\Sigma^+[P,i] \leftarrow X^2\Pi_{1/2,3/2}(000)$ vibronic transitions, i.e., from the two spin–orbit sub-

states of $X^2\Pi$ (000) to the [$P$,$i$] vibrational levels of the $A^2\Sigma^+$ state, as indicated in Figure 6. Most of which were observed for the first time. Even though the Fermi interaction in the electronic ground $X^2\Pi$ state have been extensively investigated in previous works [43,49,52-54], there has been no report in the literature about the Fermi interaction in the excited $A^2\Sigma^+$ state. Moreover, to the first-order approximation, the vibrational excitation of an odd quantum of $V_2$ is forbidden in the linear $A^2\Sigma^+ \leftarrow X^2\Pi$ (000) electronic transition [50,52,54]. As showed in Fig. 6, the forbidden bands with $\Delta V_2 = \pm 1$ are observed with considerable intensities despite their small Franck–Condon factors. This may be due to the high dissociation probabilities of the $A^2\Sigma^+$ state.

With the global fit to the observed vibronic bands, the spectral constants of the $A^2\Sigma^+$ state were determined and the results are listed in Table I. The Fermi-interaction constant $K_{122}$ was determined, for the first time, to be 21.6±1.5 $cm^{-1}$. The differences between the calculated and observed vibrational values of the $A^2\Sigma^+$ state are less than 6 $cm^{-1}$, which should be acceptable for the vibrationally resolved spectrum. The spectral constants reported in literatures are also listed in Table I. Since in previous studies the anharmonic effect as well as the Fermi-resonance interaction were not considered due to the insufficient number of spectral data of the $A^2\Sigma^+$ state, our determined vibrational frequencies are certainly different from those in literatures, especially the value of $\nu_2$. Furthermore, since many vibronic bands were identified in our PHOFEX spectrum, our spectral assignment should be more reliable, and the determined vibrational frequencies, the anharmonic constants and the Fermi-interaction constant should be in turn more precise.

### VI-2. The channel switching effect in photodissociating N2O+ ion

In Figure 7 shows the variation of total released kinetic energy [57] with the excitation photon energy determined from the simulation of $NO^+$ TOF profile, and the net TOF broadening $(\Delta t)^2 - (\Delta t_0)^2$ (opened circle) caused by its recoil velocity along the TOF axis. Here $\Delta t$ represents the width of TOF profile, and $\Delta t_0$ the width of instrumental profile. It is interesting to note that, at excitation energy around 32 000 $cm^{-1}$ (λ~312.5 nm), $\langle E_{total} \rangle$ decreases abruptly from ~8000 $cm^{-1}$ to ~1600 $cm^{-1}$ in a excitation energy range of ~250 $cm^{-1}$. With further increase of the excitation energy, $\langle E_{total} \rangle$ increases almost linearly from 1600 $cm^{-1}$ to 4000 $cm^{-1}$

**TABLE I.** Spectral constants of $N_2O^+$ ($A^2\Sigma^+$) determined from the global fit of the PHOFEX spectrum with consideration of Fermi-resonance interactions. All the values in the table are given in unit of $cm^{-1}$.

| | | References | | | | |
|---|---|---|---|---|---|---|
| Our work | | Ref.55 | Ref. 43 | Ref. 56 | Ref. 50 | Ref. 48 |
| $\nu_1$ | 1380.9±3.1 | 1358 -5.82 | 1345.52 | 1360±15 | 1346 | |
| $\nu_2$ | 627.3±1.8 | | 614.1 | 2470±15 | 614 | |
| $\nu_3$ | 2433.0±7.4 | | 2451.7 | | 2452 | |
| $\chi_{11}$ | -8.0±0.9 | | | | | |
| $\chi_{22}$ | -0.4±0.2 | | | | | -1.4[a] |
| $\chi_{33}$ | -11.8±4.0 | | | | | |
| $\chi_{12}$ | -13.1±1.1 | | | | | |
| $\chi_{23}$ | -3.6±0.9 | | | | | |
| $K_{122}$ | 21.6±1.5 | | 28 229.94 | | | |
| $T_0$ | 28230±1 | | | | | |
| Spin–orbit splitting | | | | | | |
| $X^2\Pi_{3/2,1/2}$ | 133.8±1.0 | | 132.36 | 130 | | |

[a]Estimated value.

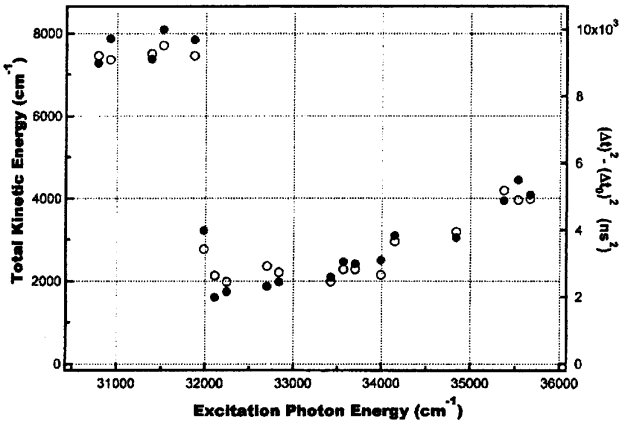


**Figure 7:** Variation of total released kinetic energy (solid circle) with the excitation photon energy determined from the simulation of $NO^+$ TOF profile, and the net TOF broadening $(\Delta t)^2 - (\Delta t_0)^2$ (opened circle) caused by its recoil velocity along the TOF axis. $\Delta t$ represents the width of TOF profile, and $\Delta t_0$ the width of instrumental profile. The abrupt and deep decrease of total kinetic energy at ~32 000 $cm^{-1}$ indicates that a new dissociation channel is opened and plays a dominant role in a narrow excitation energy region.

at excitation energy of 35 500 $cm^{-1}$. Such a sudden drop in $<E_{total}>$ cannot be attributed to the increase of $NO^+$ internal energy. Since the vibrational frequency of $NO^+(X^1\Sigma^+)$ is 2 376 $cm^{-1}$ and energy gap between the lowest electronically excited state and the $X^1\Sigma^+$ state is 52 190 $cm^{-1}$, the 6400 $cm^{-1}$ decrease in $<E_{total}>$ implies an increase of 2–3 vibrational quantum numbers of $NO^+$ ($^1\Sigma^+$). It is unlikely that such an abrupt change occurs in an excitation energy range of merely 250 $cm^{-1}$. The only possibility is that a new dissociation channel with a higher limit has been opened suddenly and becomes the main dissociation pathway.

It is known that there are two dissociation limits to produce $NO^+$ fragment in the present studied wavelength range, i.e., $NO^+$ $(X^1\Sigma^+)$+N($^4$S) at 10430 $cm^{-1}$ (Channel A), and $NO^+$ $(X\ ^1\Sigma^+)$+N($^2D$) at 29660 $cm^{-1}$ (Channel B)[43]. Therefore, the already opened channel at low excitation energy region should be Channel A, and the newly opened channel at around 32 000 $cm^{-1}$ should be Channel B. Since the dissociation limit of Channel B is much higher than that of Channel A, as long as Channel B is opened, the total released kinetic energy from this channel will decrease remarkably, causing the decrease of measured $<E_{total}>$. Furthermore, the decrease of $<E_{total}>$ from ~8000 $cm^{-1}$ to ~1600 $cm^{-1}$ indicates that the contribution of Channel A should not exceed 20%, meaning that Channel B replaces Channel A and becomes the main dissociation pathway. Further analysis shows that the dissociation pathway changes completely from Channel A to Channel B at excitation energy around 32 000 $cm^{-1}$. This implies that Channels A switches to Channel B at around 32 000 $cm^{-1}$. The dissociation channel switching process occurs in an excitation energy range of ~250 $cm^{-1}$.

This switching effect was attributed to the competition between the two dissociation channels. All previous works regarding the dissociation mechanism concentrated mainly at low excitation energy regions corresponding to dissociation Channel A. The dissociation mechanism for Channel A has been well established by previous theoretical studies [58,59]. The $A^2\Sigma^+$ state first couples with the bound $1^4\Pi$ state via

spin-orbit interaction, the latter couples to the repulsive $1^4\Sigma^-$ state, and finally leads to $NO^+$ ($X^1\Sigma^+$) and $N(^4S)$ fragments. Therefore, the dissociation rate is governed by the weak spin-orbit coupling strength between the $A^2\Sigma^+$ and the $1^4\Pi$ states. For the dissociation Channel B, since it correlates to the adiabatic dissociation limit of the ground state $X\,^2\Pi$ of $N_2O^+$ [54], it must originate from the dissociation in the $X^2\Pi$ state. As indicated by Dehmer *et al.* [ 54] and Chen *et al.* [50], and also as shown in our spectroscopic study of $N_2O^+$( $A^2\Sigma^+$) [42], the $A^2\Sigma^+$ state can also interact with the $X^2\Pi$ state via vibronic coupling, although this interaction can not lead to the dissociation via Channel B in previously studied low excitation energy range. But if energetically allowed, the $A^2\Sigma^+$ state would dissociate due to the coupling with the $X^2\Pi$ state, leading to the dissociation via Channel B.

In linear geometries, since the $A^2\Sigma^+$ and $X^2\Pi$ states differ by one spin orbital, and their vibronic coupling strength would be distinctly larger than that between the $A^2\Sigma^+$ and $1^4\Pi$ states, which differs by two spin orbitals. Therefore, if energetically allowed, the dissociation rate from the $X^2\Pi$ state (Channel B) should be much larger than that from the $1^4\Pi$ and $1^4\Sigma^-$ states (Channel A). This means that dissociation from Channel B should be much more competitive than that from Channel A, and that Channel B should replace Channel A to become the dominant dissociation pathway. Since for the dissociation Channel B, $N_2O^+$ ( $A^2\Sigma^+$) has less time to redistribute its total available excess energy among the internal degrees, the kinetic energy partition ratio must be larger than that for Channel A, as confirmed from our analyses. Our observed dissociation channel switching position (~32 000 $cm^{-1}$) is roughly 2340 $cm^{-1}$ higher than the threshold energy of Channel B. This could be attributed to the existence of a potential barrier along the N–$NO^+$ bond stretching at the state, as predicted by Chambaud *et al* [59].

## VII. Summary and the expectation for further study

The studies of three typical molecular ions, $CS_2^+$ with $D_{\infty h}$ symmetry, $SO_2^+$ with $C_{2v}$ symmetry, and $N_2O^+$ with $C_{\infty v}$ symmetry, by using two-color laser method have been reviewed.

The first dissociation channel $S^+(^4S)$+$CS(X^1\Sigma^+)$ and the second dissociation channel $CS^+(X^2\Sigma^+)$+$S(^3P)$ of $CS_2^+$ molecular ions have been investigated by measuring the photofragment $S^+$ and $CS^+$ excitation (PHOFEX) spectrum in the wavelength range of 385–482 nm. The [1+1] photodissociation process of $CS_2^+$ ion was suggested by the PHOFEX spectrum in above wavelength region, where the $CS_2^+$ ions were prepared purely by [3+1] REMPI of $CS_2$ at 483.2 nm. The PHOFEX spectrum was assigned completely as the $CS_2^+$ ($\tilde{A}\,^2\Pi_u$) ←$CS_2^+$ ($\tilde{X}\,^2\Pi_g$) transition. The adiabatic appearance potential of the $CS^+$ ion was determined to be 5.852±0.005eV above the $\tilde{X}\,^2\Pi_{g,3/2}$ (0,0,0) level of the $CS_2^+$ ion. The product branching ratios ($CS^+/S^+$), as measured from the PHOFEX spectra increases from 0 to slightly larger than 1 in the range of 47200-50400 $cm^{-1}$ (two photon energy). The dissociation mechanism to obtain $S^+$ and $CS^+$ from $CS_2^+$ was discussed and was preliminarily attributed to (i) $CS_2^+$ ($\tilde{X}\,^2\Pi_g$) → $CS_2^+$ ($\tilde{A}\,^2\Pi_u$) through one-photon excitation, (ii) $CS_2^+$ ($\tilde{A}\,^2\Pi_u$) → $CS_2^+$ ($\tilde{X}^\dagger$) via an internal conversion process (because of the vibronic coupling between the Ã state and the $\tilde{X}$ state, which enhances the efficiency of the second excitation step), (iii) $CS_2^+$ ($\tilde{X}^\dagger$ ) → $CS_2^+$ ($\tilde{B}\,^2\Sigma_u^+$ ) through the second photon excitation, and (iv) $CS_2^+$ ($\tilde{B}\,^2\Sigma_u^+$ ) → $S^+(^4S)$+$CS(X^1\Sigma^+)$ and $CS_2^+$ ($\tilde{B}\,^2\Sigma_u^+$ ) → $CS^+(X\,^2\Sigma^+)$+$S(^3P)$, because the energy curve crossing with the repulsive $^4\Sigma^-$ state and/or $^2\Sigma^-$ state correlated with the first and the second dissociation limits.

By preparing $SO_2^+$ molecular ions via [3+1] multiphoton ionization of the neutral $SO_2$ molecules at 380.85nm, the photodissociation process and the symmetry of the excited states of $SO_2^+$ molecular ions has been investigated by measuring the photofragment $SO^+$ excitation spectrum in UV (282-332 nm) and visible (562-664 nm) wavelength. The PHOFEX spectrum in the UV range was assigned essentially to the $SO_2^+$ ($\tilde{E},\tilde{D}$) ←$SO_2^+$ ($\tilde{X}\,^2A_1$) transitions. The transitions from $\tilde{X}\,^2A_1$ (000) to the bend vibration levels of $SO_2^+$ ($\tilde{D}$) were suggested. The lower $\nu_2$ of ~240 $cm^{-1}$ for $\tilde{D}$ state, given by us, in comparison with $\nu_2$ of ~360 $cm^{-1}$ for $\tilde{C}$ state, given by photoelectron spectrum (*3,4*), means that the potential curve of the $\tilde{D}$ state is not similar to other states along the bend vibrational coordinate. The symmetry of the $\tilde{D}$ state of $SO_2^+$ was determined as $\tilde{D}^2B_2$. Around $\tilde{D}$ states there should be a repulsive state of symmetry $\alpha^2A_2$ converge to the dissociation limit of $SO^+(X^2\Pi)$+$O(^3P_g)$, and the

predissociation of $SO_2^+$ ($\tilde{D}$) comes from the coupling between $\tilde{D}$ and $\alpha^2A_2$ repulsive state.

The spectroscopic studies of the $A^2\Sigma^+$ state of $N_2O^+$ ions were shown. Pure parent ions of $N_2O^+$ at the $X^2\Pi_{1/2,3/2}(000)$ level, were prepared by [3+1] REMPI of neutral $N_2O$ molecules at 360.55 nm, and were excited to various vibrational levels of the $A^2\Sigma^+$ state by a tunable laser. The PHOFEX spectrum in the wavelength range of 278–328 nm was attributed completely to the $A^2\Sigma^+ \leftarrow X^2\Pi$ electronic transition of $N_2O^+$, in which most vibronic bands were observed for the first time. By considering the Fermi resonance between the $\nu_1$ and $\nu_2$ modes, the spectrum was assigned, and the spectral constants of the $A^2\Sigma^+$ state, such as vibrational frequencies, anharmonic constants and Fermi interaction constant, were obtained with relatively high reliability and precision.

The dissociation process of $N_2O^+$ at the $A^2\Sigma^+$ state in the energy range of 30500–36000 $cm^{-1}$ has been investigated. From the TOF profiles of $NO^+$ fragment, the total released kinetic energies $<E_{total}>$ at different excitation wavelengths were roughly determined. $<E_{total}>$ is about 8000 $cm^{-1}$ at lower excitation energies, drops abruptly to 1600 $cm^{-1}$ at around 32000 $cm^{-1}$, and increases gradually with excitation energy above 32000 $cm^{-1}$. Analysis showed that at energies below ~32000 $cm^{-1}$ the dissociation pathway is $NO^+$ ($X^1\Sigma^+$)+N($^4S$) (Channels A), and at energies above ~32000 $cm^{-1}$ the dissociation pathway is $NO^+(X\ ^1\Sigma^+)$+N($^2D$) (Channel B). Channel A switches completely to Channel B at ~32000 $cm^{-1}$ in an excitation energy range of merely ~250 $cm^{-1}$. The dissociation via Channel A is indirect, the $A^2\Sigma^+$ state is slowly predissociated by a bound $1^4\Pi$ state as intermediate state via spin-orbit coupling, the latter is then coupled to a repulsive $1^4\Sigma^-$ state. The dissociation via Channel B is caused by the vibronic coupling between the $A^2\Sigma^+$ state and the $X^2\Pi$ state. The dissociation channel switching is attributed to the overwhelming dissociation rate via the $A^2\Sigma^+/X^2\Pi$ coupling over that via the $A^2\Sigma^+/1^4\Pi$ interaction at energies necessary for the opening of Channel B.

For the further study with state selected of molecular ions, it is interesting to prepare the vibrationally excited groun electronic state, for example, the (010) level of $SO_2^+$, and then to get the PHOFEX spectrum from this vibrationally excited level. We can also use the rotationally resolved level of molecular ions, such as $H_2S^+$, to study the rotationally resolved PHOFEX spectrum. In the case of that the fragment ions in multiphoton ionization produced by ionization laser cannot be avoided, the improvement of this technique can be used to get the PHOFEX spectrum produced only by dissociation laser. For example, a shift in time and in space in the lasers-molecules interaction zone between the first and the second laser pulses permitted the mass selective detection of the secondary fragments, produced by dissociation laser, and their discrimination against primary fragment ions, produced by ionization laser, of the same mass by using a time of flight analyzer [25] [60].

## ACKNOWLEDGMENTS

We would like to thank our colleagues, especially Dr. Zhong Wang and Dr. Haifeng Xu, for their contribution to the research results quoted in this paper.

Supports from the National Natural Science Foundation of China (#20173053, #20273063 and #20373067) and National Key Basic Research Special Foundation research program (#G1999075304) is gratefully acknowledged.

## REFERENCES

1. Hudson, R. D., 1970, Rev. Geophys. Space Phys., 9, 305.
2. Forney, D. Kellogg, C. B. Thompson, W. E. and Jacox, M. E. 2000, J. Chem. Phys., 113(1), 86.
3. Pons, M., Joubert, O., Matinet, C., Pelletier, J., Panabiere, J.-P., and Weill, A., 1994, Jpn. J. App. Phys. 33, 991.
4. Burley, J. D., Evin, K. M., and Armentrout, P. B., 1987, J. Chem. Phys. 86, 1944.
5. Komiha, N., 1994, J. Mol. Struct. 306, 313.
6. Baer, T., 1979, in "Gas phase ion chemistry", Vol.1, ed. M. T. Bowers, Academic, New York, Ch.5, p.153.
7. Dutuit, O., 1991, in "Fundamentals of Gas phase ion chemistry", ed. K. R. Jennings, Kluwer Academic Publishers, Printed in the Netherlands, p.21-54.
8. Marx, R., 1992, *Int. J. Mass Spectrom. Ion Phys.*, 118/119, 661.

9. Zhang, L., Chen, J., Xu, H., Dai, J., Liu, S., and Ma, X., 2001, *J. Chem. Phys.*, 114(24), 10768.
10. Baker, J., Konstantaki, M., and Couris, S., 1995, J. Chem. Phys., 103, 2436.
11. Xue, B., Chen, Y., and Dai, H.-L., 2000, *J. Chem. Phys.*, 112(5), 2210.
12. Szarka M. G., and Wallace, S. C., 1991, J. Chem. Phys., 95, 2336.
13. Scheper, C. R., Kuijt, J., Buma, W. J., and deLange, C. A., 1998, J. Chem. Phys., 109, 7844.
14. Zhang, L., Wang, F., Wang, Z., Yu, S., Liu, S., Ma, X., 2004, *J. Phys. Chem.* A, 108, 1342.
15. Callomon, J. H., 1958, *Proc. R. Soc. London, Ser. A, 244*, 220.
16. Leach, S., 1970, 1964, *J. Chim. Phys. Phys.-Chim. Biol., 61*, 1493, *67*, 74.
17. Eland, J. H. D., Danby, C. J., 1968, *Int. J. Mass Spectrom. Ion Phys., 1*, 111.
18. Brundle, C. R., Turner, D. W., 1969, *Int. J. Mass Spectrom. Ion Phys., 2*, 195.
19. Frost, D. C., Lee, S. T., McDowell, C. A., 1973, *J. Chem. Phys., 59*, 5484.
20. Frey, R., Gotchev, B., Peatman, W. B., Pollak, H., Schlag, E. W., 1978, *Int. J. Mass Spectrom. Ion Phys., 26*, 137.
21. Wang, L. S., Reutt, J. E., Lee, Y. T., Shirley, D. A., 1988, *J. Electron Spectrosc. Relat. Phenom., 47*, 167.
22. Brehm, B., Eland, J. H. D., Frey, R., Kustler, A., 1973, *Int. J. Mass Spectrom. Ion Phys., 12*, 213.
23. Danis, P. O., Wyttenbach, T., Maier, J. P., 1988, *J. Chem. Phys., 88*, 3451.
24. Evard, D. D., Wyttenbach, T., Maier, J. P., 1989, *J. Phys. Chem., 93*, 3522.
25. Hwang, W. G., Kim, H. L., Kim, M. S., 2000, *J. Chem. Phys., 113*, 4153.
26. Momigny, J., Mathieu, G., Wankenne, H., 1973, *Chem. Phys. Lett., 21*, 606.
27. Morgan, R. A., Baldwin, M. A., Orr-Ewing, A. J., Ashfold, M. N. R., Buma, W. J., Milan, J. B., de Lange, C. A., 1996, *J. Chem. Phys., 104*, 6117.
28. Balfour, W. J., *Can. J. Phys.* 1976, *54*, 1969.
29. McHale, J. L., 2002, Molecular Spectroscopy, Pearson Education North Asia Limited and Science Press, p 341.
30. Wang, Z., Zhang, L., Li, J., Wang, F., and Yu, S., 2003, J. Mol. Spectroscopy, 221,139.
31. Zhang, L., Wang, Z., Li, J., Wang, F., Liu, S., Yu, S., and Ma, X., 2003, J. Chem. Phys., 118(20), 9185.
32. Wang, L., Lee, Y. T., and Shirley, D. A., 1987, J. Chem. Phys., 87(5), 2489.
33. Holland, D. M. P., MacDonald, M. A., Hayes, M. A., Baltzer, P., Karlsson, L., Lundqvist, M., Wannberg, B., Niessen, W.von, 1994, *Chem. Phys.*, 188, 317.
34. Dujardin G., and Leach, S., 1981, *J. Chem. Phys.*, 75(6), 2521.
35. Weiss, M. J., Hsieh, Ta-Cheng and Meisels, G. G., 1979, *J. Chem. Phys.*, 71, 567.
36. Thomas, T. F., Dale, F., and Paulson J. F., 1986, *J. Chem. Phys.*, 84(3), 1215.
37. Hillier I. H., and Saunders, V. R., 1971, *Mol. Phys.*, 22, 193.
38. Brehm, B., Eland, J. H. D., Frey, R., and Kustler, A., 1973, *Int. J. Mass Spectrom. Ion Processes*, 2, 197.
39. Weiss, M. J., Hsieh, Ta-Cheng, and Meisels, G. G., 1979, *J. Chem. Phys.*, 71, 567.
40. Norwood, K., and Ng, C. Y., 1990, *J. Chem. Phys.*, 93(9), 6440.
41. Herzberg, G., *Electronic Spectra and Electronic Structures of Polyatomic Molecules* (Litton Educational, New York, 1966), pp. 248, 445.
42. Xu, H., Guo, Y., Li, Q., Liu, S., and Ma, X., 2003, *J. Chem. Phys.*, 119(22), 11609.
43. Callomon J. H., and Creutzberg, F., 1974, Philos. Trans. R. Soc. London, Ser. A 277, 157.
44. Lerme, J., Abed, S., Larzilliere, M., Holt, R. A., and Carre, M., 1986.
45. Lerme, J., Abed, S., Holt, R. A., Larzilliere, M., and Carre, M., 1983, Chem. Phys. Lett. 96, 403.
46. Larzilliere, M., Gragued, K., Lerme, J., and Koffend, J. B., 1987, Chem. Phys. Lett. 134, 467.
47. Abed, S., Broyer, M., Carre, M., Gaillard, M. L., and Larzilliere, M., 1983, Chem. Phys. 74, 9.
48. Larzillere M., and Jungen, C. H., 1989, Mol. Phys. 67, 807.
49. Cha k el Idrissi, M., Larzilliere, M., and Carre, M., 1994, J. Chem. Phys. 100,204.
50. Chen, W., Liu, J., and Ng, C. Y., 2003, J. Phys. Chem. A 107, 8086.

51. Bernath, P. F., Dulick, M., and Field, R. W., 1981, J. Mol. Spectrosc. 86,275.
52. Aarts J. F. M., and Callomon, J. H., 1982, Chem. Phys. Lett. 91,419.
53. Fellows C. E., and Vervloet, M., 2001, Chem. Phys. 264, 203.
54. Dehmer, P. M. Dehmer, J. L. and Chupka, W. A. 1980, J. Chem. Phys. 73,126.
55. Frey, R. Kakoschke, R. and Schlag, E. W. 1982, Chem. Phys. Lett. 93, 277.
56. Frey, R. Gotchev, B. Poatman, W. B. Pollak, H. and Schlag, E. W. 1978, Chem. Phys. Lett. 54, 411.
57. Xu, H. Guo, Y. Li, Q. Shi, Y. Liu, S. and Ma, X. 2004, *J. Chem. Phys.*, 121(7), 3069.
58. Beswick J. A. and Horani, M. 1981, Chem. Phys. Lett. 78,4.
59. Chambaud G. *et al.*, 2000, Mol. Phys. 98, 1793.
60. Boesl, U., Neusser, H. J., and Schlag, E. W., 1982, Chem. Phys. Lett. 87, 1.